Special quasirandom structures description of the local structure of disordered Bi_{0.5}K_{0.5}TiO₃

Bo Jiang^{1,2}, De-Ye Lin³, Xin Wang⁴, Sverre M. Selbach^{1*} and Katharine Page^{2,4*},

¹Department of Materials Science and Engineering, NTNU – Norwegian University of

Science and Technology, 7491 Trondheim, Norway.

²Neutron Scattering Division, Oak Ridge National Laboratory, Oak Ridge, TN 37830, USA.

³CAEP software Center for High Performance Numercial Simulation, Institute of Applied

Physics and Computational Mathematics, Huayuan road 6, Beijing 100088, P.R. China

⁴Department of Materials Science and Engineering, University of Tennessee, Knoxville, TN 37996, USA.

*Correspondence should be addressed to selbach@ntnu.no and kpage10@utk.edu

Abstract

Polar nanoregions (PNRs) are believed to play a decisive role in the local and macroscopic polarization in relaxor ferroelectrics. The limited microscopic understanding of the structure and dynamics of PNRs hampers the rational design of new lead-free materials. Here, the local structure of A-site disordered $Bi_{0.5}K_{0.5}TiO_3$ (BKT) is investigated using synchrotron X-ray and neutron pair distribution function (PDF) analysis and density functional theory (DFT) optimized special quasirandom structures (SQS). DFT relaxed SQS with $4\times4\times4$ supercell size can reproduce the experimental PDFs of disordered BKT, as well as the partial PDFs and total polarization, with comparable results to those reported from combined analysis of X-ray and neutron PDF data with large-box Reverse Monte Carlo (RMC) methods. We find that small

Bi³⁺-rich polar clusters are likely to be the microscopic origin of relaxor behavior in disordered BKT, and that the existence of large polar nanoregions (PNRs) is not necessary to explain the relaxor properties. Our results also highlight the great potential of the SQS approach to gain nanoscale to microscopic understanding of other relaxor solid solutions.

1. INTRODUCTION

The relaxor ferroelectric Bi_{0.5}K_{0.5}TiO₃ (BKT) and its solid solutions with various other perovskite structures are candidates for replacing environmentally hazardous Pb(Zr,Ti)O₃ (PZT) in many piezoelectric applications ¹⁻⁵. BKT exhibits relaxor-like behavior of broad dielectric peaks with frequency-dependent temperatures of maximum permittivity ⁶⁻⁸. Like Pb²⁺ in PZT, Bi³⁺ possesses a 6s² lone electron pair which greatly enhances the polarization⁹⁻¹¹. The average structure of BKT is tetragonal P4mm (a = 3.933 Å, c=3.975 Å, c/a=1.01)¹² at room temperature ^{2,13-16}, is pseudo-cubic above a T_2 of around 270-310 °C, , and is paraelectric with cubic $Pm \overline{3}$ m structure above the Curie temperature T_C of 370-410 °C ^{2,14,15,17,18}. The A-site sublattice in BKT is disordered with no superstructure peaks due to cation ordering, although the difference in radii and formal charge between Bi³⁺ (1.31 Å) and K⁺ (1.65 Å, 21% larger) is large¹⁹. Our previous investigation of the local and average structure of BKT from room temperature to above T_C suggests that local polar regions partly cancel each other below T_C , and completely average out above T_C ^{20,21}, consistent with other reports. ^{22,23}

Polar nanoregions (PNRs) have been proposed to emerge below the Burns temperature T_D in relaxors 13,24 , and these PNRs are believed to increase in size upon further cooling. PNRs are difficult to detect by conventional in-house X-ray diffraction (XRD) because of their small size on the order of a few lattice constants 25 , and their origin and existence has been debated 26,27 . Several studies have inferred the presence of PNRs or polar domains in BKT using XRD,

transmission electron microscopy (TEM) and dielectric characterization, but no direct experimental evidence has been presented 6,18,28 . Pair distribution functions (PDFs) from synchrotron X-ray and time-of-flight neutron total scattering can probe the local and intermediate range structure of amorphous and disordered materials $^{22,29-34}$. PDFs are particularly useful for characterizing disordered relaxor ferroelectrics $^{20,21,35-38}$, and the first direct observation of PNRs was accomplished by total scattering studies of Pb(Mg_{1/3}Nb_{2/3})O₃ 39 . Levin *et al.* 22 first reported polar cation displacements (PNR size ≈ 2 nm) in BKT supercell models produced via simultaneous fitting of neutron/X-ray total scattering and extended X-ray absorption fine-structure (EXAFS) data in Reverse Monte Carlo (RMC) refinements, but the evidence provided for correlated displacements in their RMC results was limited to visual inspection of a projection of Bi³⁺ atom column displacements. Evidence for PNRs above ≈ 2 nm in size was not demonstrated in a quantitative manor. 40

Here we investigate the local structure of Bi_{0.5}K_{0.5}TiO₃ by a combination of synchrotron X-ray and neutron total scattering measurements and density functional theory (DFT) calculations using special quasirandom structures (SQS) ⁴¹. The SQS approach allows design of periodic supercells representative of a real disordered state, and has been shown to successfully reproduce electronic and thermodynamic properties in disordered alloys ⁴²⁻⁴⁴; it has only been applied to a few perovskite oxide systems to date ⁴⁵⁻⁴⁷. We compare the total and partial experimental PDFs with computed PDFs from RMC modelling and DFT relaxed SQS with different cell sizes. We are able to infer the existence of Bi³⁺-rich polar clusters rather than classic polar nanoregions (PNRs) as the origin of relaxor behaviour in disordered BKT, with smaller models and fewer data sets.

2. EXPERIMENTAL AND COMPUTATIONAL DETAILS

Phase pure BKT was prepared by conventional solid state reaction as described in our previous

work ^{20,21}. Synchrotron X-ray and neutron total scattering were performed at beamline ID22 (λ = 0.199965 Å, 62 keV) at the European Synchrotron Radiation Facility (ESRF) and the NOMAD instrument⁴⁸ at the Spallation Neutron Source (SNS) at Oak Ridge National Laboratory, respectively. Synchrotron X-ray and neutron total scattering data G(r) were reduced with the PDFgetX3 software ⁴⁹ and ADDIE software⁵⁰, respectively, and subsequently analyzed by small-box modeling using PDFgui ⁵¹ and by large-box Reverse Monte Carlo (RMC) modeling using RMCprofile ⁵² (details are given in the Supporting Information).

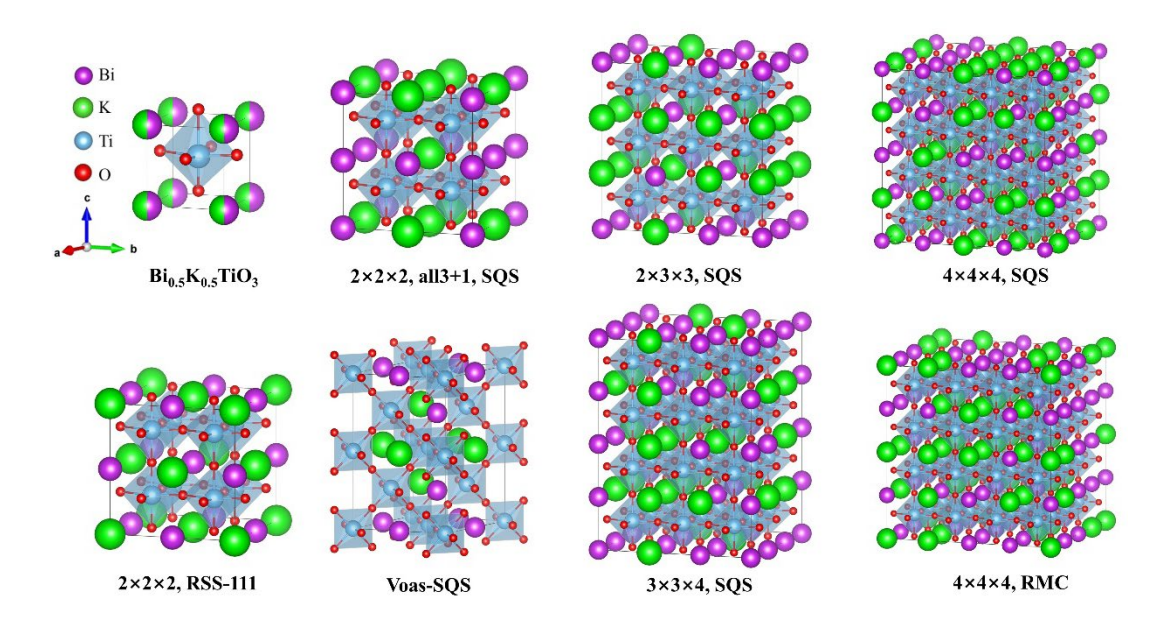


Figure 1. The Bi_{0.5}K_{0.5}TiO₃ (BKT) structure models used in this work, with Bi, K, Ti and O atoms shown as purple, green, blue and red spheres, respectively. TiO₆ octahedral units are highlighted with blue shading. The models from left to right represent a randomly mixed A-site BKT with 5 atoms per unit cell, a 2×2×2 cation rock salt 111 ordered structure with 40 atoms per unit cell (2×2×2, RSS-111), a 2×2×2 'all3+1' structure (SQS) with 40 atoms²¹, the SQS model with relaxed lattice vector from Voas *et al.* ⁴⁶ with 40 atoms per unit cell, a 2×3×3 SQS model with 90 atoms, a 3×3×4 SQS model with 180 atoms, a 4×4×4 SQS model with

320 atoms and a 4×4×4 RMC generated configuration with 320 atoms (see text for further descriptions).

The SQSs ⁴¹ of BKT were prepared with the mcsqs utility in the Alloy Theoretic Automated Toolkit (ATAT) 53,54 . Starting with the 5 atoms perovskite unit cell Bi_{0.5}K_{0.5}TiO₃, a $2\times2\times2$ SQS model with 40 atoms, a $2\times3\times3$ SQS model with 90 atoms, a $3\times3\times4$ SQS model with 180 atoms, and a $4 \times 4 \times 4$ SQS model with 320 atoms were generated with unrelaxed lattice vectors, as shown in Figure 1. The Metropolis Monte Carlo algorithm was applied in ATAT to randomly exchange the cation atomic positions ⁵⁴. The optimal SQS was selected as the one with the minimum deviation from the completely random pairwise and triplet correlations to 3rd-nearest (3NN) distance (the one closest matching a disordered solid solution arrangement given the fixed number of atoms for each finite supercell size). It should be noted that more than one SQS configuration was generated for each supercell, and only the one resulting in the most random cation configuration was used in this study. The correlation functions of the generated SQSs are listed in Table S1, and the atomic positions of the generated SQSs are given in Table S2. The randomly mixed A-site structure with 5 atoms, and the 2×2 ×2 cation rock salt 111 ordered structure ^{20,21} are also compared in this study, shown alongside the SQS models in Figure 1. Note that the SQS for the $2\times2\times2$ supercell corresponds to the 'all3+1' structure cation ordered perovskite model (featuring alternating layers of 3:1 and 1:3 K:Bi ratios). Finally, the SQS superlattice of 40 atoms with relaxed lattice vector from Voas et al. 46 which describes the K_{0.5}Na_{0.5}NbO₃ solid solution (KNN) is also examined in this work (by replacing Na and Nb atoms with Bi and Ti atoms, respectively).

Density functional theory (DFT) calculations were performed with the *Vienna Ab initio* Simulation Package (VASP) code ^{55,56} using the PBEsol functional ^{57,58}. The standard PBE

PAW potentials Bi_d (5d¹⁰6s²6p³), K_sv (3s²3p⁶54s¹), Ti_pv (3p⁶3d²4s²) and O (2s²p⁴) supplied with VASP were used. Brillouin zone integrations were done on a 3×3×3 mesh of k points for the 2×2×2 supercell (40 atoms), a 3×2×2 mesh of k points for the 2×3×3 supercell (90 atoms), and a gamma mesh of k-points for the 3×3×4 supercell and 4×4×4 supercell (180 atoms and 320 atoms, respectively) in this work. A plane wave cutoff energy of 550 eV was used and all the structures were relaxed until the forces on the atoms fell below 0.01 eV/Å. All the structure models in Figure 1 were relaxed by DFT, except the mixed A-site BKT model with only 5 atoms.

3. RESULTS AND DISCUSSION

The synchrotron X-ray PDF (xPDF) and neutron PDF (nPDF) in Figure 2 are first compared with calculated PDFs from all the structure models in Figure 1. All the calculated PDFs were obtained by applying a small equivalent isotropic atomic displacement (U_{iso}) value equal to 0.005 Å² to simplify visual comparison with the experimental PDF. The PDF from the mixed A-site P4mm model has sharper peaks than the PDFs from the other models, including some peaks (~3.7 Å in xPDF) not found in the measured xPDF where atomic displacement parameters and local atomic displacements in real BKT broaden the PDF peaks 21 .

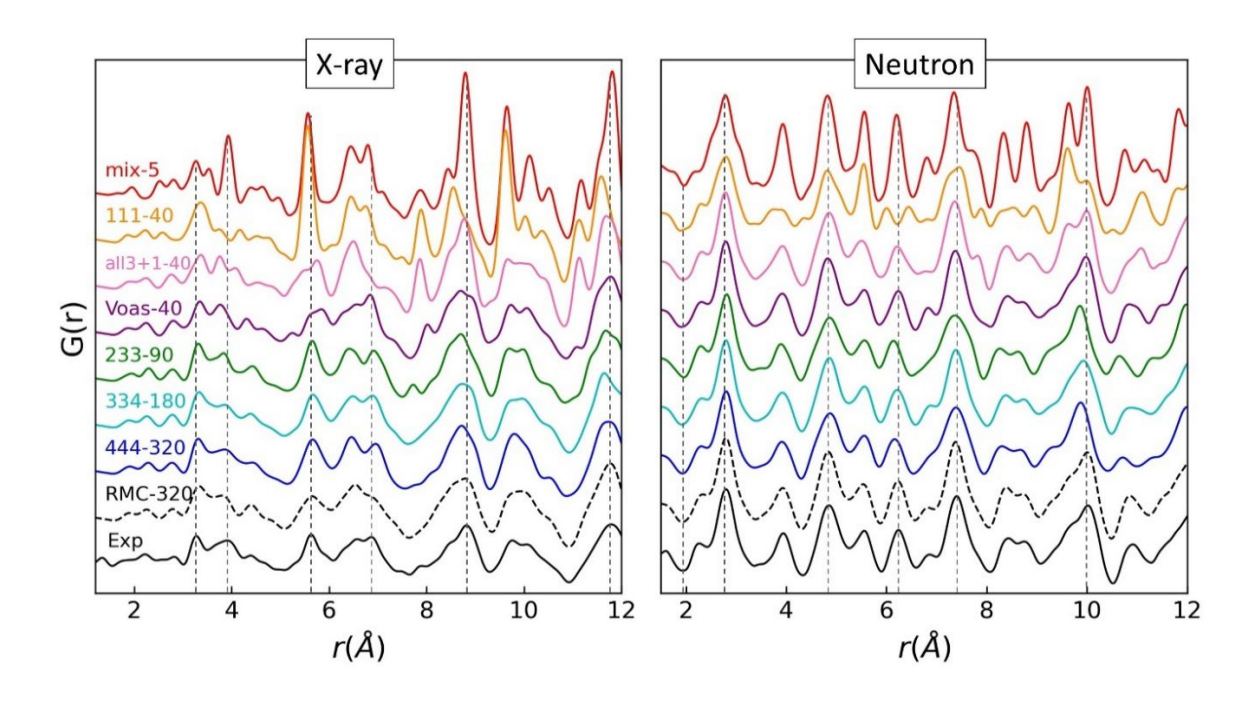


Figure 2. Comparison of experimental synchrotron X-ray and neutron PDFs (solid black lines) of BKT with PDFs calculated from the structural models shown in Figure 1 using $U_{iso} = 0.005$ Å². The simulated PDFs are labelled according to the model names in Figure 1 as "name-x," where x is the number of atoms in the structural model. The dotted dash lines represent a guide to the eye for some dominant peak positions observed in the experimental PDFs.

When comparing xPDFs and nPDFs calculated from the 2×2×2 rock salt 111 and all3+1 structures, we find that the all3+1 configuration gives a better agreement with the relative intensities of the experimental peaks than the 111 configuration (note the peaks at ~5.5 Å and ~10 Å for xPDFs and ~4 Å and 6.2 Å for nPDFs). The PDF computed from the SQS model derived from the work of Voas *et al.* ⁴⁶ has greater similarity to the experimental PDF, featuring reduced peak intensities at ~7 Å and 11 Å in the X-ray case and ~9.5 Å in the neutron case. However, several unmatched peaks remain. The PDFs calculated from 2×3×3 SQS, 3×3×4 SQS and 4×4×4 SQS supercells show improved agreement with the experimental PDFs with respect to peak positions and relative intensities. The PDF calculated from a structure model first refined by RMC and then relaxed by DFT gives excellent agreement with the experimental

PDF, demonstrating the ability of RMC to model the disordered structure of BKT (see Figure S1).

To further study the size and configuration effects among different models, co-refinements were performed against X-ray and neutron PDF datasets with each model using PDFgui, 51 with an identical number of refined parameters fit for all models: scale factors, lattice constants, correlated atomic motion parameter (delta2) and equivalent isotropic U_{iso} values as refined variables. make the number of refined parameters identical The refined results are shown in Table S3 and Figure S2, in which both the 111 and all3+1 40 atoms structures exhibit poor goodness-of-fit (R_w) values due to their artificial long-range cation ordering, while the fit using the randomly mixed A-site BKT structure produces a fair R_w value. This result is consistent with previous findings supporting a random distribution of Bi and K cations at the local scale. ²⁰⁻²³ It is noteworthy that the neutron PDF is well-fit by the 40 atom structure from Voas *et al*. with relaxed lattice vector, while poor agreement is observed for synchrotron X-ray PDF fits. This suggests that a small SQS is not capable of capturing the accurate local and intermediate range structure of this relaxor material, similar to observations for other systems ⁴⁵. The local A-site cation configuration motif ²¹ may thus exist over an extended length scale in BKT, necessitating larger supercell models.²³ We can see that the introduction of larger SQS models with $2\times3\times3$, $3\times3\times4$ and $4\times4\times4$ supercells can significantly improve the fits for both xPDF and nPDF, demonstrating the ability of larger supercells to reproduce the real structure of BKT. Note that the 4×4×4 SQS model gave the best agreement with the experimental PDFs, with only a negligible mismatch at $r = \sim 3.8 \text{ Å} - 4 \text{ Å}$ for the xPDF fit.

The corresponding partial PDFs (pPDFs) resulting from co-refinement of experimental xPDF and nPDF fits with the 4×4×4 SQS model are depicted in Figure 3, clearly identifying the nature of atomic pair peaks. Since Ti has a negative neutron scattering length (-3.438 fm), the

atomic pairs containing Ti (Bi-Ti, K-Ti, and Ti-O) in neutron pPDFs appear as valleys instead of peaks. It is noteworthy that the O-O pairs show much larger intensity due to the large neutron scattering length of oxygen atoms (5.803 fm) compared to the X-ray scattering atomic form factor value (4.089 fm)⁵⁹. In contrast, the Bi-Bi, Bi-K and Bi-Ti neutron pair correlations have much lower intensities than corresponding X-ray peaks, meaning that X-ray PDF is more suitable for modeling Bi related pairs (i.e., 62.425 fm Bi³⁺, 10.977 fm K⁺ and 13.198 fm Ti⁴⁺).⁵⁹ Note that the Bi-Ti peak at ~ 3.8 Å in the X-ray PDF is still not well described, presumably due to the limitations of the 4×4×4 SQS model to both fit the significant local distortion (evident at ~3.8 Å) and average out the resulting local lattice strains in all directions (evident in higher-r PDF).²¹ It should be noted that the O-containing pairs (O-O, Ti-O, Bi-O and K-O) contribute most strongly to nPDF data, while the local ordering/disordering in BKT mainly comes from the mixed A-site of Bi³⁺ and K⁺. This explains why the small 40 atoms model from Voas et al. with relaxed lattice vector can simulate the nPDF data much better than the xPDF data. The comparative analysis indicates the importance of combining refinements using synchrotron X-ray and neutron PDF data to probe the local structure of complex oxides, as observed previously by others. ²²

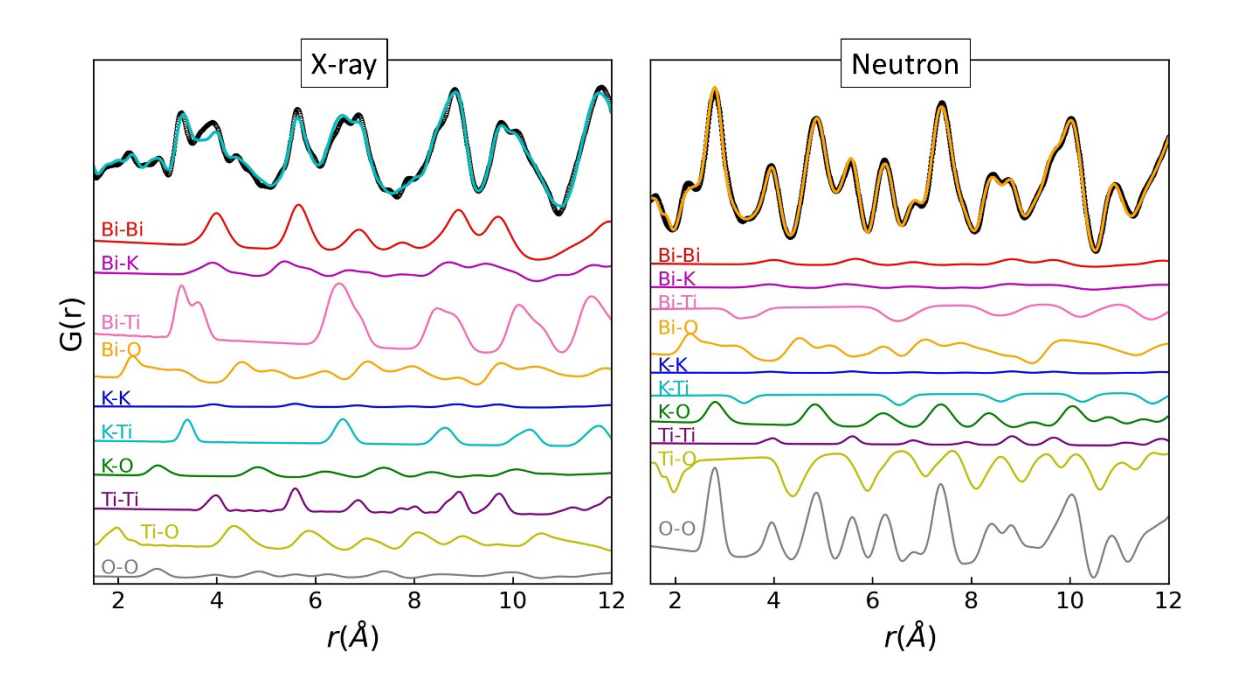


Figure 3. Comparison of the experimental synchrotron X-ray and neutron PDFs of BKT (black circles), shown with fits and corresponding labelled pPDF contributions from the 4×4×4 SQS DFT-relaxed model results from PDFgui analysis.

We further performed the large-box RMC refinements to individual synchrotron X-ray and neutron PDFs, then simultaneously to both X-ray and neutron PDFs. Figure 4 compares selected partial PDFs from RMC refinements and compares them to partial xPDFs simulated with the 4×4×4 SQS model using PDFgui. The three distinct peaks below 4 Å in the Bi-O bond distribution from xPDF analysis alone are consistent with previous PDF and ab initio molecular dynamics (AIMD) studies²⁰⁻²², but an unexpected peak around ~2.5 Å was observed. The Bi-O bond distribution in nPDF analysis alone results in a broad second peak, which possiblyresults from mis-modeling overlapping O-O intensities (~2.8 Å). The co-refinement of X-ray and neutron PDFs yields a much better Bi-O bond distribution landscape compared to the result from the 4×4×4 SQS DFT-relaxed model. The same trends were observed in K-O and Bi-Ti bond distributions, where a significantly broadened peak results for K-O by xPDF analysis alone due to the smaller X-ray scattering strength of K⁺ and O²⁻. It is noteworthy that the unexpected peak around ~2.8 Å by xPDF (reported in our previous xPDF paper^{20,21} due to the O-O overlapping peak) disappeared after introducing the nPDF to RMC refinement, in agreement with the result from the 4×4×4 SQS DFT-relaxed model. The K-Ti peaks resulting from the fits to different datasets exhibit similar bond distributions because of the distinct Xray and neutron scattering factors for K⁺ and Ti⁴⁺. These results reveal that the supercell SQS can provide not only average structure models, but also reveal local structure information for BKT. The BKT structure model generated from RMC captures disorder from thermal disorder, site disorder and lattice distortions, tending to produce the most disordered structure that is consistent with the data. Thus, we conclude from the partial PDF distribution analysis that the

combined use of x-ray and neutron PDF in RMC refinements in complex perovskite oxide solid solutions provides improved modeling of the local structure. Meanwhile, the SQS using relatively large supercell models after DFT relaxation has demonstrated its capability of reproducing the experimental PDF for predicting the local structure.

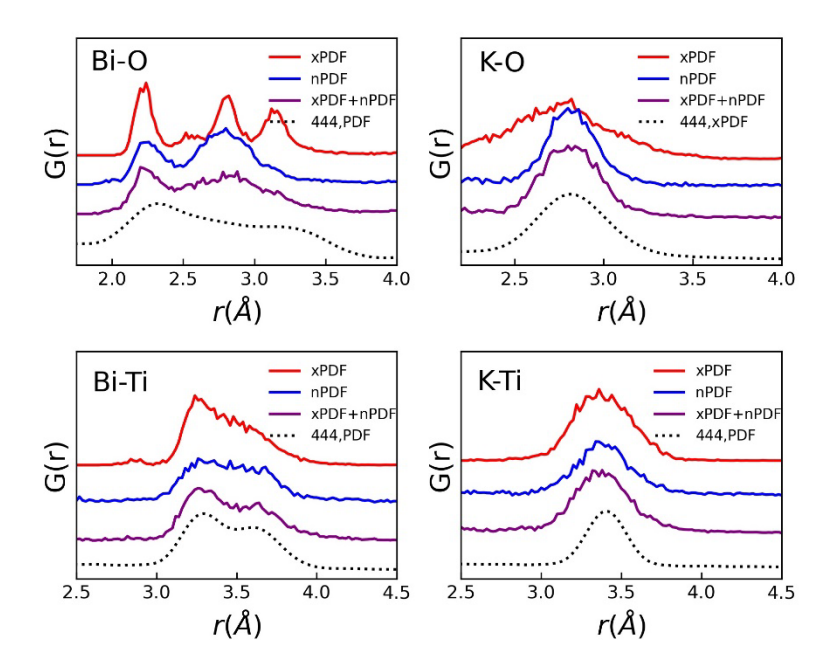


Figure 4. Selected partial PDF distribution for Bi-O, K-O, Bi-Ti and K-Ti pair correlations from RMC refinements to synchrotron X-ray PDF (red), neutron PDF (blue), and a combination of X-ray and neutron PDFs (purple). The dashed line corresponds to the partial xPDFs simulated from the 4×4×4 SQS model refined with PDFgui analysis.

It is challenging to evaluate the possible existence and role of polar nanoregions (PNRs) in BKT. Hitherto, no direct evidence of PNRs in BKT has been obtained from PDFs or other experiments $^{6,18,20-22}$. A possible reason for this is the obvious difficulty of unambiguously identifying tetragonal PNRs in an on-average tetragonal lattice. The spontaneous polarization P_s calculated by a point charge model for BKT configurations of different sizes is shown in Figure 5(a). The lattice parameters of supercell $2\times3\times3$ SQS, $3\times3\times4$ SQS, and $4\times4\times4$ SQS were fixed to experimental values to calculate the spontaneous polarization. The relaxed all3+1 and

111 configurations yield a large total P_s of more than ~50 μ C/cm². The P_s of 2×3×3 SQS, 3×3×4 SQS, and 4×4×4 SQS models gradually decrease with increasing supercell size, with the P_s of 4×4×4 SQS model resulting in good agreement with the range of reported experimental values indicated with grey shading in Figure 5(a) ^{14,15,60}. Note that the maximum P_s , value along the x, y, z directions ([001], [010], and [100] directions) is strongly dependent on the A-site cation configuration, implying that the local polar regions partly cancel each other out over larger length scales ^{20,21}.

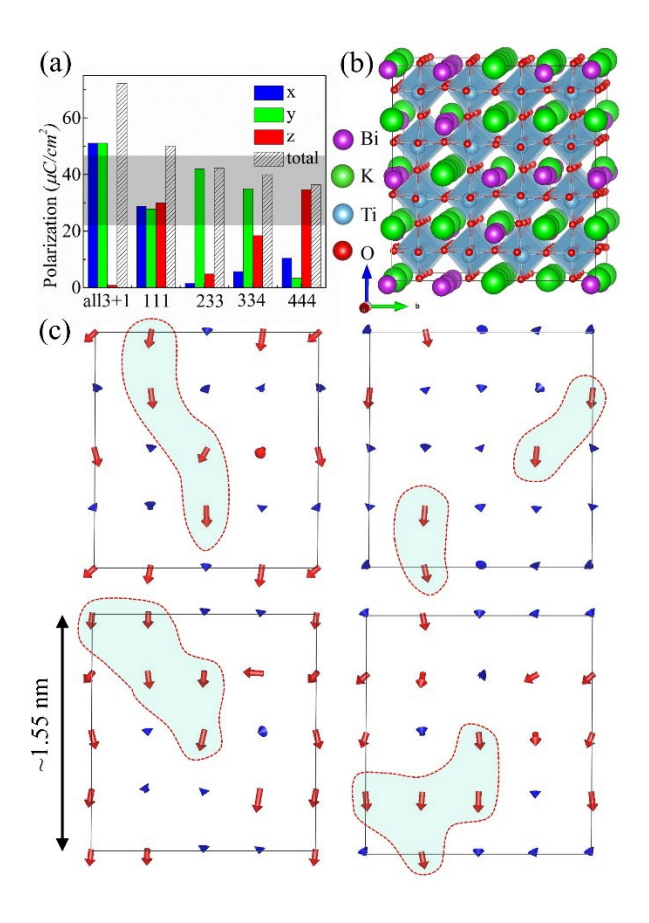


Figure 5. (a) Polarization (P_s) from point charge model for different configurations of BKT where the blue, green, red and shaded bars represent x, y, z and total polarizations, respectively. The range of reported experimental values [12, 13, 56] is represented with grey shading. (b) Structure of the $4 \times 4 \times 4$ SQS model after geometry optimization by DFT. (c) Dipole configurations from four layers in the yz-plane of the $4 \times 4 \times 4$ SQS optimized model. Blue and

red arrows denote the actual (not normalized) polar displacement vectors of K⁺ and Bi³⁺, respectively, with respect to their average positions.

The final structure after geometry optimization by DFT for the 4×4×4 SQS model is shown in Figure 5(b), where the tetragonal distortions of the Ti-O octahedra are visible. The corresponding dipole configurations from four layers in the yz-plane in the relaxed 4×4×4 SQS model are depicted in Figure 5(c) to elucidate the local polarization mechanism. We note that K⁺ ions have small displacements from their high symmetry positions, while the majority of Bi³⁺ ions show larger displacements, particularly along the z axis. The local dipole configurations are in good agreement with the proposed 3D BKT model at room temperature in our previous work ²⁰. Some of the clusters of parallel Bi³⁺ dipoles can be described as polar clusters or regions, as previously reported in BZT 61. Recent studies have proposed that the PNRs are responsible for the grain size dependence of the phase transition temperature of BKT ^{6,28}. Nevertheless, no direct experimental evidence of PNRs in BKT, e.g. like in PMN from PDFs analysis ³⁹, have been found. The relaxor behavior of BKT can be viewed as intrinsic, caused by disordered A-site configurations yielding local Bi³⁺-rich polar clusters. These results suggest the displacement field for Bi column projections in previous work from Levin et al.²² (which were qualitiatively identified through visual inspection and not assigned a distinct length scale or degree of correlation) may be overestimated. Specifically, it is not clear whether the size of polar clusters in that work approach the threshold of PNRs. In our findings, larger PNRs are thus not necessary to explain the relaxor behavior of disordered BKT.

4. CONCLUSION

To summarize, we have examined the local structure of the disordered Bi_{0.5}K_{0.5}TiO₃ relaxor ferroelectric by DFT calculations using the special quasirandom structures (SQS) approach combined with X-ray and neutron pair distribution function (PDF) analysis. By constructing

different size and configuration models, we have demonstrated that the local atomic structure of A-site disordered BKT can be captured with appropriate SQS models and with fewer experimental datasets than previously demonstrated with large-box RMC methodology. Smaller SQS models (here referring to the 40 atom model from Voas *et al.*²²) capture the nPDF data well but still fail to capture the xPDF data, suggesting the need for more extended A-site configurational disorder in the BKT relaxor. The computed PDFs, partial PDFs and total spontaneous polarization P_s calculated from larger 4×4×4 SQS supercells are in good agreement with those resulting from a combination RMC refinement of X-ray and neutron PDF data. Our analysis suggests that large PNRs are not necessary to explain the relaxor behaviour of BKT due to the inherent presence of Bi³⁺-rich polar clusters. In short, the results from this combined approach demonstrate great potential for using the SQS approach to provide in depth understanding of relaxor solid solutions and other highly disordered systems.

DEDICATION

Many women have contributed to the field of ferroelectrics and flamed interest in their complex crystallography, beginning with Helen Megaw's determination of the structure of BaTiO₃ in 1945.⁶² We dedicate this article to women who have worked / are working towards uncovering the roles of local structure and chemical ordering in relaxor ferroelectric ceramics, including Pam A. Thomas, Jing Zhu, and Michelle Dolgos.

SUPPLEMENTARY MATERIAL

See the supplementary material for the details of SQS results, PDFgui refinements and RMC modelling.

ACKNOWLEDGMENTS

This work was supported by the Research Council of Norway through the SYNKNØYT project 228571/F50. Work by K.P. was funded by the National Science Foundation (DMR-2145174). This research used the NOMAD beamline at the Spallation Neutron Source, a DOE Office of Science User Facility operated by the Oak Ridge National Laboratory. Computational resources were provided by the Uninett Sigma2 through the project NN9264K and the VirtuES project as well as the Compute and Data Environment for Science (CADES) at Oak Ridge National Laboratory which is supported by the Office of Science of the U.S. Department of Energy under Contract No. DE-AC05-00OR22725. We thank Andrew Fitch for his valuable assistance at beamline ID22 at ESRF.

DATA AVAILABILITY

The data that support the findings of this study are available within the article and its supplementary material.

REFERENCES

- Y. Saito, H. Takao, T. Tani, T. Nonoyama, K. Takatori, T. Homma, T. Nagaya, and M. Nakamura, Nature **432**, 84 (2004).
- J. Rödel, W. Jo, K. T. P. Seifert, E. M. Anton, T. Granzow, and D. Damjanovic, Journal of the American Ceramic Society **92**, 1153 (2009).
- ³ V. V. Shvartsman and D. C. Lupascu, Journal of the American Ceramic Society **95**, 1 (2012).
- ⁴ H. Z. Jin and J. Zhu, Journal of Applied Physics **92,** 4594 (2002).
- D. I. Woodward, R. Dittmer, W. Jo, D. Walker, D. S. Keeble, M. W. Dale, J. Rödel, and P. A. Thomas, Journal of Applied Physics **115**, 114109 (2014).
- M. Hagiwara and S. Fujihara, Japanese Journal of Applied Physics **54**, 10ND10 (2015).
- J. F. Yang, Y. D. Hou, C. Wang, M. K. Zhu, and H. Yan, Applied Physics Letters **91**, 023118 (2007).

- ⁸ Z. F. Li, C. L. Wang, W. L. Zhong, J. C. Li, and M. L. Zhao, Journal of Applied Physics **94,** 2548 (2003).
- ⁹ Y. D. Hou, L. Hou, J. F. Yang, M. K. Zhu, H. Wang, and H. Yan, Acta Chimica Sinica **65**, 950 (2007).
- J. Konig, M. Spreitzer, B. Jancar, D. Suvorov, Z. Samardzija, and A. Popovic, Journal of the European Ceramic Society **29**, 1695 (2009).
- ¹¹ I. Krad, O. Bidault, N. Geoffroy, and M. E. L. Maaoui, Ceramics International **42**, 3751 (2016).
- E. T. Wefring, M. I. Morozov, M.-A. Einarsrud, and T. Grande, Journal of the American Ceramic Society **97**, 2928 (2014).
- G. Burns and F. H. Dacol, Solid State Communications **48**, 853 (1983).
- Y. Hiruma, R. Aoyagi, H. Nagata, and T. Takenaka, Japanese Journal of Applied Physics **44**, 5040 (2005).
- Y. Hiruma, H. Nagata, and T. Takenaka, Japanese Journal of Applied Physics **46**, 1081 (2007).
- M. Otonicar, S. D. Skapin, M. Spreitzer, and D. Suvorov, Journal of the European Ceramic Society 30, 971 (2010).
- V. V. Ivanova, Kapyshev, A.G., Venevtsev, Yu.N., Zhdanov, G.S., Bull. Acad. Sci. USSR Phys. Ser. **26**, 358 (1962).
- M. Otonicar, S. D. Skapin, B. Jancar, R. Ubic, and D. Suvorov, Journal of the American Ceramic Society **93**, 4168 (2010).
- ¹⁹ R. D. Shannon, Acta Crystallographica Section A **32**, 751 (1976).
- B. Jiang, T. Ræder, D.-Y. Lin, T. Grande, and S. M. Selbach, Chemistry of Materials **30**, 2631 (2018).
- B. Jiang, T. Grande, and S. M. Selbach, Chemistry of Materials **29**, 4244 (2017).
- I. Levin, D. S. Keeble, G. Cibin, H. Y. Playford, M. Eremenko, V. Krayzman, W. J. Laws, and I. M. Reaney, Chemistry of Materials 31, 2450 (2019).
- M. K. Niranjan, P. K. Kumari, K. Banerjee, and S. Asthana, Journal of Applied Physics **123**, 244106 (2018).
- ²⁴ F. Li, S. J. Zhang, Z. Xu, and L. Q. Chen, Advanced Functional Materials **27**, 1700310 (2017).
- J. Macutkevic, J. Banys, A. Bussmann-Holder, and A. R. Bishop, Physical Review B **83**, 184301 (2011).
- M. E. Manley, J. W. Lynn, D. L. Abernathy, E. D. Specht, O. Delaire, A. R. Bishop, R. Sahul, and J. D. Budai, Nature Communications **5**, 9 (2014).
- ²⁷ G. Y. Xu, J. S. Wen, C. Stock, and P. M. Gehring, Nature Materials **7**, 562 (2008).
- M. Hagiwara and S. Fujihara, Applied Physics Letters **107**, 012903 (2015).
- E. Aksel, J. S. Forrester, J. C. Nino, K. Page, D. P. Shoemaker, and J. L. Jones, Physical Review B **87**, 104113 (2013).
- V. A. Shuvaeva, D. Zekria, A. M. Glazer, Q. Jiang, S. M. Weber, P. Bhattacharya, and P. A. Thomas, Physical Review B **71**, 174114 (2005).
- ³¹ V. Petkov, Materials Today **11,** 28 (2008).
- V. Petkov, S. M. Selbach, M. A. Einarsrud, T. Grande, and S. D. Shastri, Physical Review Letters **105**, 185501 (2010).
- ³³ C. M. Culbertson, A. T. Flak, M. Yatskin, P. H. Y. Cheong, D. P. Cann, and M. R. Dolgos, Scientific Reports **10**, 3729 (2020).
- D. S. Keeble, E. R. Barney, D. A. Keen, M. G. Tucker, J. Kreisel, and P. A. Thomas, Advanced Functional Materials **23**, 185 (2013).
- ³⁵ C. A. Young and A. L. Goodwin, Journal of Materials Chemistry **21**, 6464 (2011).
- D. A. Keen and A. L. Goodwin, Nature **521**, 303 (2015).
- D. Hou, C. Zhao, A. R. Paterson, S. Li, and J. L. Jones, Journal of the European Ceramic Society **38**, 971.
- ³⁸ B. Jiang, D.-Y. Lin, T. Grande, and S. M. Selbach, Acta Materialia **177**, 222 (2019).

- I. K. Jeong, T. W. Darling, J. K. Lee, T. Proffen, R. H. Heffner, J. S. Park, K. S. Hong, W. Dmowski, and T. Egami, Physical Review Letters 94, 147602 (2005).
- J. Hlinka, Journal of Advanced Dielectrics **2**, 1241006 (2012).
- A. Zunger, S. H. Wei, L. G. Ferreira, and J. E. Bernard, Physical Review Letters **65**, 353 (1990).
- A. van de Walle, G. Ceder, and U. V. Waghmare, Physical Review Letters **80**, 4911 (1998).
- G. Ghosh, A. van de Walle, and M. Asta, Acta Materialia **56,** 3202 (2008).
- ⁴⁴ K. C. Hass, L. C. Davis, and A. Zunger, Physical Review B **42**, 3757 (1990).
- ⁴⁵ Z. J. Jiang, Y. Nahas, B. Xu, S. Prosandeev, D. W. Wang, and L. Bellaiche, Journal of Physics-Condensed Matter **28**, 13 (2016).
- B. K. Voas, T. M. Usher, X. M. Liu, S. Li, J. L. Jones, X. L. Tan, V. R. Cooper, and S. P. Beckman, Physical Review B **90**, 6 (2014).
- B. Jiang, C. A. Bridges, R. R. Unocic, K. C. Pitike, V. R. Cooper, Y. Zhang, D.-Y. Lin, and K. Page, Journal of the American Chemical Society **143**, 4193 (2020).
- J. Neuefeind, M. Feygenson, J. Carruth, R. Hoffmann, and K. K. Chipley, Nuclear Instruments and Methods in Physics Research Section B: Beam Interactions with Materials and Atoms **287**, 68 (2012).
- P. Juhas, T. Davis, C. L. Farrow, and S. J. L. Billinge, Journal of Applied Crystallography **46**, 560 (2013).
- M. T. McDonnell, D. P. Olds, K. L. Page, J. C. Neufeind, M. G. Tucker, J. C. Bilheux, W. Zhou, and P. F. Peterson, Acta Crystallographica Section A **73**, a377 (2017).
- ⁵¹ C. L. Farrow, P. Juhas, J. W. Liu, D. Bryndin, E. S. Bozin, J. Bloch, T. Proffen, and S. J. Billinge, Journal of Physics: Condensed Matter **19**, 335219 (2007).
- M. G. Tucker, D. A. Keen, M. T. Dove, A. L. Goodwin, and Q. Hui, Journal of Physics: Condensed Matter **19**, 335218 (2007).
- A. van de Walle, Calphad-Computer Coupling of Phase Diagrams and Thermochemistry **33**, 266 (2009).
- A. van de Walle, P. Tiwary, M. de Jong, D. L. Olmsted, M. Asta, A. Dick, D. Shin, Y. Wang, L. Q. Chen, and Z. K. Liu, Calphad-Computer Coupling of Phase Diagrams and Thermochemistry **42**, 13 (2013).
- ⁵⁵ G. Kresse and J. Furthmuller, Physical Review B **54**, 11169 (1996).
- ⁵⁶ G. Kresse and D. Joubert, Physical Review B **59**, 1758 (1999).
- J. P. Perdew, A. Ruzsinszky, G. I. Csonka, O. A. Vydrov, G. E. Scuseria, L. A. Constantin, X. L. Zhou, and K. Burke, Physical Review Letters **100**, 136406 (2008).
- J. P. Perdew, K. Burke, and M. Ernzerhof, Physical Review Letters **77**, 3865 (1996).
- P. A. Doyle and P. S. Turner, Acta Crystallographica Section a-Crystal Physics Diffraction Theoretical and General Crystallography **A 24**, 390 (1968).
- J. Konig and D. Suvorov, Journal of the European Ceramic Society **35**, 2791 (2015).
- A. R. Akbarzadeh, S. Prosandeev, E. J. Walter, A. Al-Barakaty, and L. Bellaiche, Physical Review Letters **108**, 5 (2012).
- ⁶² H. D. Megaw, Nature **155**, 484 (1945).

BIOGRAPHIES



Bo Jiang (he/him), Postdoctoral Associate, Neutron Scattering Division, Oak Ridge National Laboratory. His research interests include the synthesis, structural characterization and properties of complex materials, such as ferroelectric, piezoelectric, thermoelelectric, battery and high entropy materials, particularly through cutting-edge neutron and X-ray total scattering and computational modelling techniques.



De-Ye Lin (he/him), Associate Research Fellow, CAEP software Center for High Performance Numercial Simulation and Institute of Applied Physics and Computational Mathematics, China. His research interests focus on the atomic-scale modeling and simulation of materials, including structural properties, irradiation effects, mechanical properties, equation of states and some related theoretical models.



Xin Wang (she/her), Graduate Student, Department of Materials Science and Engineering, University of Tennessee, Knoxville. Her research interests include materials chemistry, complex and high entropy oxide materials, and neutron and X-ray total scattering.



Sverre M. Selbach (he/him), Professor, Department of Materials Science and Engineering, Norwegian University of Science and Technology, Trondheim, Norway. His research concerns the structure, stability, phase transitions and transport properties of complex and disordered materials. Current interests include solid-state electrolytes, ferroic domain walls and unconventional ferroics.



Katharine Page (she/her), Assistant Professor, Department of Materials Science and Engineering, University of Tennessee, Knoxville, and Joint Faculty, Neutron Scattering Division, Oak Ridge National Laboratory. Her research group works to make and understand complex functional materials, both bulk and nano, through advances in metastable synthesis routes and novel X-ray and neutron scattering methods. Current research interests include ferroelectric oxides, energy conversion materials, and nanoscale catalysts, among others.